(12)

PROGRESS REPORT

METASTABLE PHASES OF RAPIDLY SOLIDIFIED Al-RICH Al-Fe ALLOYS

D. SHECHTMAN AND E. HOROWITZ

CENTER FOR MATERIALS RESEARCH
THE JOHNS HOPKINS UNIVERSITY
G.W.C. WHITING SCHOOL OF ENGINEERING
BALTIMORE, MARYLAND 21218

(301) 338-7916

APPROVED FOR PUBLIC RELEASE
DISTRIBUTION UNLIMITED

DARPA ORDER NO: MDA 903-83-K-0400
EFFECTIVE DATE: 08-05-83
EXPIRATION DATE: 08-04-85
SPONSORED BY: DEFENSE ADVANCED RESEARCH PROJECTS AGENCY (DARPA)

JANUARY 1984

SECURITY CLASSIFICATION OF THIS PAGE (When Data Entered)

REPORT DOCUMENTATION PAGE	READ INSTRUCTIONS BEFORE COMPLETING FORM
1. REPORT NUMBER: CMR-DARPA-8	2. GOVT ACCESSION NO.: AD-A139 598
3. RECIPIENT'S CATALOG NUMBER	
4. TITLE (and Subtitle): Metastable Phases of Rapidly Solidified Al-Rich Al-Fe Alloys	5. TYPE OF REPORT & PERIOD COVERED: Progress Report 9-1-83 to 1-1-84
	6. PERFORMING ORG. REPORT NUMBER
7. AUTHOR(s): D. Shechtman and E. Horowitz	8. CONTRACT OR GRANT NUMBER(s): MDA-903-83-K-0400
9. PERFORMING ORGANIZATION NAME AND ADDRESS: The Johns Hopkins University Center for Materials Research Baltimore, Maryland 21218	10. PROGRAM ELEMENT, PROJECT, TASK AREA & WORK UNIT NUMBERS
11. CONTROLLING OFFICE NAME AND ADDRESS: DARPA 1400 Wilson Blvd, Arlington, Va 22209	12. REPORT DATE: January 1984
	13. NUMBER OF PAGES: 53
14. MONITORING AGENCY NAME & ADDRESS (if different from Controlling Office): ONRRR George Washington University 2110 G Street SW Washington, D. C. 20037	15. SECURITY CLASS. (of this report): A
	15a. DECLASSIFICATION/DOWNGRADING SCHEDULE

16. DISTRIBUTION STATEMENT (of this Report)

Approved for public release, distribution unlimited.

17. DISTRIBUTION STATEMENT (of the abstract entered in Block 20, if different from Report)

18. SUPPLEMENTARY NOTES

19. KEY WORDS (Continue on reverse side if necessary and identify by block number)

rapidly solidified alloys, aluminum rich/aluminum-iron alloys.

20. ABSTRACT (Continue on reverse side if necessary and identify by block number)

This report covers an investigation of the Al-rich, Al-Fe alloys prepared by the rapid solidification procedure and characterized using transmission electron microscopy and nuclear gamma-ray resonance.

DD FORM 1 JAN 73 1473 EDITION OF 1 NOV 65 IS OBSOLETE

TABLE OF CONTENTS

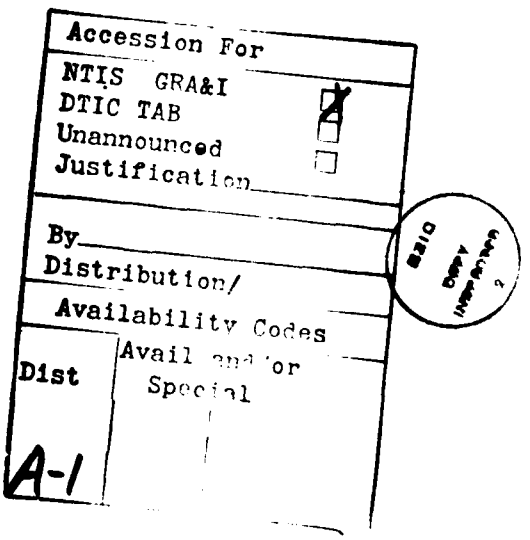

LIST OF TABLES

LIST OF FIGURES

LIST OF FIGURES

LIST OF FIGURES

LIST OF FIGURES

EXECUTIVE SUMMARY

As part of a continuing investigation on the characterization of rapidly solidified alloys, the present report describes the results of the study of the various phases observed in rapidly solidified aluminum rich, aluminum-iron alloys. Two experimental techniques, transmission electron microscopy (TEM) and nuclear gamma-ray resonance (NGR) were used to obtain valuable data and information on the microstructure and composition of selected alloys. While papers in the literature deal with Al-Fe alloys, these have largely been concerned with alloys having relatively low iron concentrations. The aluminum alloys described in this report cover a broad range of iron concentrations and consist of samples in the Fe 1 weight percent to 34 weight percent range. The interesting features of the microstructure are discussed also in these terms. Aluminum-iron alloys with 18 weight percent Fe were subjected to a series of heat treatments in order to evaluate the thermal stability of the phases. Special care has been exercised in reproducing the microphotographs in order to preserve for the reader the unique microstructural details captured in the original observations.

I. Introduction

Because of the current and potential technological importance of metastable phases in aluminum alloys, rapid solidification of aluminum rich alloys is being extensively studied. We report here a study of the Al-rich Al-Fe alloys, investigated using transmission electron microscopy (TEM) and nuclear gamma-ray resonance (NGR). This work was done in cooperation with L.J. Swartzendruber of the NBS Metallurgy Division who performed the NGR experiments. In the region up to about 25 atomic percent Fe, current phase diagrams [1] indicate the existence of two stable phases, namely primary α-Al (with a minute amount of iron in solid solution) and Al_3Fe. Rapid solidification of Al-Fe alloys within the composition range of these two phases produces a number of metastable phases which always accompany the Fcc Al phase. Which particular phases form depends on the composition and on the solidification rate. The following phases have been reported: (a) Al_6Fe [2-3], (b) Al_9Fe_2 [4], (c) Al_mFe [5] and (d) Al_xFe [6]. Several review papers summarize the information available on rapidly solidified Al-Fe alloys [7-9]. According to Young and Cline [6] the various phases which occur in Al-Fe alloys with less than about 0.9 a/o Fe can be put in the following order of increasing cooling rate: Al_3Fe, Al_xFe, Al_6Fe, Al_9Fe_2, Al_mFe. Compositions for this study were selected to extend the previous results to higher iron concentrations, and up to Al-20 a/o.

II. Experimental

The alloys were rapidly solidified by chill block casting on a spinning copper wheel in an inert atmosphere. The ribbons obtained were approximately 2mm wide and 0.035 to 0.050 mm thick. Thin foils for transmission electron microscopy were prepared using a jet electropolishing unit and standard electrolyte at -40°C. All the ribbons were studied in a transmission electron microscope (TEM). The information obtained included general images of the phase structure, selected area microdiffractions, and x-ray microanalysis of the composition of the main phases. Samples for nuclear gamma-ray resonance (NGR) were prepared by cutting the ribbons into 6 mm lengths and placing them side by side to form a square approximately 6 mm on a side. The resulting samples had an areal density of ^{57}Fe between 0.05 and 0.1 mg/cm^2. The nominal composition of the alloys under study are given in Table 1.

weight % Fe	1	2	3	9	10	11	12	14	16	18	25.7	34
atomic % Fe	0.485	0.976	1.47	4.56	5.09	5.64	6.18	7.29	8.61	9.59	14.1	19.93

TABLE 1: The Composition of the Alloys Under Study

The alloy Al-18 wt% Fe was subjected to a series of heat treatments in order to study the transformations and coarsening of the various phases. Specimens of these alloys were also studied by TEM and NGR.

1. TEM Results

a. General (As Spun Alloys)

At 25 w/o Fe (Al_6Fe) and below, the following phases were found in the melt-spun alloys: α-Al solid solution with less than 1 w/o Fe, and an "S" phase with a composition near that of Al_6Fe. The diffraction pattern of the observed "S" phase does not appear to match the diffraction patterns for any of the previously reported aluminum-rich phases (Al_3Fe, Al_xFe, Al_6Fe, Al_9Fe_2, or Al_mFe) [2,3]. An additional flower-shaped phase was detected in the alloy Al-18 wt% Fe in small quantities.

Below 9 w/o, a cellular solidification structure is observed. The cells consist of α-Al solid solution and the cell boundaries of the "S" phase. At a composition between 9 and 10 w/o Fe a change in morphology of the melt-spun structure occurs. Above 10 w/o, a coarse primary globular "S" phase appears, imbedded in the cellular structure. The globular phase appears to have a crystal structure and a composition identical to the "S" phase at the cell boundaries. At compositions above 25 w/o Fe, Al_3Fe is formed along with the globular "S" phase.

b. Phase Analysis

The rapidly solidified Al-Fe ribbons which contain up to 34 wt% Fe (19.93 at%) were found to contain the following phases.

(1) Supersaturated Fcc aluminum

The degree of supersaturation as determined by microstructural observations is probably a little less than 1 wt%. This is a lower degree of supersaturation than previously reported by other investigators and may result in a slower cooling rate of the melt spinning technique used in this study. We believe, however, that this is not the case and that the methods used by others to determine supersaturation are sometimes misleading. All the alloys examined by us, including the alloy Al-1 wt% Fe are composed of a cellular aluminum matrix, in which the cell boundaries are significantly richer in the solute Fe. In alloys of high Fe concentration such as Al-25.7 wt% Fe and Al-34 wt% Fe, the cellular matrix does not form since other phases occupy almost the entire volume of the ribbon.

(2) The intercellular phase (the "S" phase)

The composition of the cell boundaries is difficult to determine because of the fineness of the particles in it. The analysis that was made by x-ray energy dispersion in the TEM indicated that the iron concentration in the cell boundary particles is close to 25 wt%.

The particle sizes of the intercellular "S" phase vary between the thickness of the boundary (0.1μm) to subnanometer. This is demonstrated in the characteristic ring diffraction pattern (Fig. 1). A dark field image of the intercellular

phase is shown in Fig. 2. The fineness of the intercellular "S" particle may be appreciated by observing the higher magnification dark field (Fig. 3). The nomenclature "S phase" was selected to differentiate this previously unidentified phase from other phases reported before in this system.

(3) The globular "S phase"

This phase appears in rapidly solidified alloys within the composition range Al-10 wt% Fe to Al-25 wt% Fe. The lower limit of its occurrence is a little less than 10 wt% since the phase was not detected in the alloy Al-9 wt% Fe. The upper limit may very well be higher than the one given here, but we know that it does not occur in the alloy Al-34 wt% Fe.

An example of this phase is given in Fig. 4 and a higher magnification in Fig. 5. This globular phase yields the same ring diffraction pattern as the grain boundary "S" phase (Fig. 6) and was therefore also given the nomenclature "S phase." The similarity between the cell boundary "S" phase and the globular "S" phase can be further illustrated in Figs. 7 and 8, which are bright and dark field images of the structure of the alloy Al-18 wt% Fe, respectively. The dark field image was taken from the strongest ring in the diffraction pattern and clearly both the intercellular "S" phase and the globular "S" phase are illuminated. Note also the fineness of the particles in the globular "S" phase.

The crystallographic characteristics of this phase were found to be different for various particles. In addition to the structure just described, some S phase globules are single crystals and a convergent beam diffraction pattern from such a particle is shown in Fig. 9. Other than the diffraction patterns the appearance and composition of the particles are identical. We therefore conclude that the larger crystals of the globular "S" phase represent a more stable structure, yet still metastable as described in the section on heat treatment.

The chemical composition of this phase as determined by x-ray energy dispersive analysis in the TEM is about 25 wt% Fe. This observation is also supported by the fact that the structure of the ribbon Al-25.7 wt% Fe is almost entirely composed of globular "S" particles as will be shown later.

The nature of the formation of the globular "S" phase may be the key to the understanding of the solidification process in aluminum alloys rich in iron. Our understanding of the sequence of the formation of the phases can be summarized as follows: An iron rich phase ($\sim$25 wt%) is probably the first to solidify, forming globules of "S" phase. The iron poor liquid solidifies later and has the characteristic cellular structure that forms a matrix for the globules. In this way, the already solid "S" globules can serve as nucleation sites for the growth of cellular aluminum. Examples of such events will be shown later.

Floating in the turbulent still liquid matrix, the distribution of the "S" globules may end up being irregular, i.e., coalescence of globules in one region and absence in other regions. This phenomenon will also be shown later in this report.

(4) The flower-like phase

An example of this phase is given in Fig. 10 and a diffraction pattern is shown in Fig. 11. The phase was detected only in the alloy Al-18 wt% Fe, and is relatively rare in that alloy. It has, however, a very interesting crystallography, and the same crystallography is very abundant in Al-Mn alloys of concentration higher than Al-18 wt% Mn. In these alloys the volume fraction of the phase of crystallographically identical phase is very high. The characteristics of the crystallography of this alloy will be discussed when the Al-Mn alloys of high Mn concentration are reported.

2. Microstructure of the Alloys

The Al-1 wt% Fe alloy is characterized by a cellular microstructure (Fig. 12). The cell size is between 0.5 and 1 μm and the cell boundary is decorated with dislocations. The cells are relatively free of particles and dislocations and the amount of the cell boundary phase is too small to be observed in the electron diffraction pattern (Fig. 13).

In other regions of the ribbons cell formation is not observed possibly due to a higher solidification rate. In these regions round particles 500 Å in diameter are observed (Fig. 14). The formation of these particles can be linked to the stability of the solidifying front as observed in the alloy Al-2 wt% Fe (Fig. 15). In this example the solidifying front reaches instability and the front from which cell formation is observed is seen in the center of the figure. This Al-2 wt% Fe alloy contains clearly another phase at the cell boundaries, and these are not decorated by dislocations as it is in the Al-1 wt% Fe alloy.

The alloy Al-3 wt% Fe is similar to the Al-2 wt% Fe alloy except for the thickness of the cell boundaries (Fig. 16). In this alloy the electron diffraction pattern contains rings (Fig. 17) that are diffracted from the second phase in the cell boundary and from the particles within the grains.

The alloy Al-9 wt% Fe is cellular with cell size of about 60 nm. The cell boundaries contain the "S" phase as can be seen in Figs. 1,8 and 19. The ring diffraction pattern is formed by very small particles at the cell boundaries (see also Fig. 2). The fineness of these particles is demonstrated in the dark field, Fig. 3, in which the size of the diffracting volumes within the cell boundary is as small as 1 nm.

In the Al-10 wt% Fe, the microstructure is cellular with globular "S" phase (Fig. 20). The cell size is about

20 nm while the "S" particles are about 100 nm in diameter. The globular "S" phase does not occur in alloys with less than 10 wt% Fe.

For Al-11 wt% Fe, the globular "S" phase particles are of the size of up to 200 nm and the cell size is also larger than that of the alloy containing 10 wt% fe (Fig. 4). The diffraction pattern from this microstructure contains the same rings as that of lower iron composition indicating the similarity between the structure of the cell boundary phase and that of the globular "S" phase. This result is supported by the NGR measurements. Another observation in alloys containing globular "S" particles is the fact that they can serve as nucleation sites. In this case they sometimes cluster together and cells are observed to emanate from them (Fig. 21). This is additional evidence that the globular "S" phase is the first to nucleate from the liquid.

The microstructure of Al-12 wt% Fe and Al-14 wt% Fe is similar to that of the alloy containing 11 wt% Fe. In the diffraction pattern (Fig. 22), however, the rings diffracted from the "S" phase are partially composed of discrete spots, indicating that the "S" phase crystals are larger than those found in alloys of lower Fe concentrations (Fig. 23).

As the Fe concentration increases, the cell boundary phase is composed of larger crystals. In some cases the aluminum and the cell boundary phase grow as two continuous interlocking crystals. This is demonstrated in Al-16 wt% Fe

(Fig. 24) which shows a dark field image of the cell boundary phase. In this alloy too, the globular "S" serves as a nucleation site. This occurs either on each particle individually or on particle clusters (Fig. 25).

The globular "S" phase in the alloy Al-18 wt% Fe averages 50 nm in diameter and contains the usual cellular structure between the globular particles (Fig. 7). There are regions, however, in this alloy in which the density of the particles is high and no cell formation is observed (Fig. 26). In such cases, the particle size is normally below average. A dark field image, taken from the brightest ring in the diffraction pattern (Fig. 6) indicates that the "S" phase, either in the cell boundaries or in the globular form contains large quantities of microcrystallites (Fig. 8). The ribbon of this composition also contains particles which are not observed in alloys of lower Fe concentration. This phase has a characteristic flower shape (Fig. 10) and diffraction patterns obtained from it (Fig. 11) are identical to ones which were obtained from metastable phases in Al-Mn and Al-Cr alloys, indicating a similar crystallography. The analysis of this phase, which is abundant in these alloys but rather rare in the Al-Fe alloys will be performed and reported elsewhere.

The globular "S" phase Al-25.7 wt% Fe (Fe_6Al) has the size of 250 nm on the average, and its volume fraction approaches 100% in certain regions (Fig. 27). Cells are only rarely observed and the particles are flower-like in shape

(Fig. 28). All other characteristics of the particle seem to be identical to the alloys of lower Fe concentration.

The analysis of the microstructure of the ribbon containing Al-34 wt% Fe composition yielded only one phase (Fig. 29) analyzed as Al_3Fe by its diffraction pattern (Fig. 30).

3. Thermal Stability of the Phases

In order to study the stability of the phases in the alloys a series of heat treatments was performed on the alloy Al-18 wt% Fe. Ribbons for the heat treatment were sealed by Vycor tubes in vacuum better than 10^{-6} Torr. The tubes were treated at 300°C for 10 hours, at 400°C for 1 and 8 hours and at 500°C for 1 and 6 hours. Following 10 hours at 300°C no morphological changes could be detected. However, the globular "S" yields better contrast in the microscope and each globule seems to have recrystallized into one crystal (Fig. 31), as opposed to the microcrystalline nature of the non-heat treated S particles. At 400°C following 1 hour the first indication of phase transformation can be found. The transformation products are fine elongated particles, probably Al_3Fe as can be seen in Fig. 32. In the case of another speciman treated for 8 hours at this temperature the transformation is completed and the characteristic striated morphology of the Al_3Fe particles are found everywhere within the alloy (Fig. 33). The heat treatment that was performed

at 500°C resulted only in the coarsening of the Al_3Fe particles, some of which reach the size of a few microns (Fig. 34).

4. Nuclear Gamma-Ray Resonance (NGR)

a. General

Nuclear gamma-ray resonance (NGR) spectra were obtained for the rapidly solidified alloys containing 1,2,3,9,12,18, 25.7, and 34 w/o Fe, and 19 w/o alloys isothermally annealed at temperatures up to 600°C. Spectra from these samples are shown in Fig. 35. All spectra were taken at room temperature. Because the NGR spectrum from the various phases in iron-rich iron-aluminum alloys are known to overlap to a considerable extent[10], the analysis of the spectra obtained for the rapidly solidified alloys of this study is not straightforward. However, a consistent interpretation can be obtained by analyzing the spectra as shown in Fig. 36. The spectra are least squares fitted to three lines (as shown in Fig. 35). The lines are assumed to be Lorentzian in shape with two parameters, a full width at half maximum (FWHM) and a peak position which is measured with respect to the center of a pure α-Fe spectrum at room temperature. The three fitted lines are interpreted as arising from a doublet, D, a central singlet, S1, and a singlet, S2, which lies under one of the doublet peaks. Numerical results are given in Table 2. The doublet splitting is the separation between the outer two lines. The doublet

TABLE 2

Parameter obtained from least squares analysis of the NGR spectra using the analysis as described in the text. Numbers shown to only two decimal places were constrained to those values during the analysis.

Fe Fraction		Heat	Doublet D				Central Singlet S1			Singlet S2		
w/o	a/o	Treatment	Splitting mm/sec	Isomer shift mm/sec	FWHM mm/sec	Area frac.	Isomer shift mm/sec	FWHM mm/sec	Area frac.	Isomer shift	η mm/sec	Area frac.
1	0.485	none	0.422	0.205	0.335	0.746	0.21	0.23	0.022	0.40	0.27	0.23
2	0.976	none	0.400	0.208	0.334	0.804	0.21	0.23	0.032	0.40	0.27	0.16
3	1.47	none	0.388	0.206	0.328	0.916	0.21	0.23	0.056	0.40	0.27	0.02
9	4.56	none	0.372	0.215	0.292	0.951	0.21	0.23	0.049	0.40	0.27	<0.02
12	6.18	none	0.390	0.195	0.348	0.983	0.21	0.23	0.017	0.40	0.27	<0.02
18	9.59	none	0.396	0.196	0.344	0.976	0.21	0.23	0.024	0.40	0.27	<0.02
25.7	14.1	none	0.375	0.190	0.332	0.918	0.21	0.23	0.082	0.40	0.27	<0.02
34	19.9	none	0.386	0.209	0.312	0.758	0.208	0.241	0.242	0.40	0.27	<0.02
18	9.59	10 hr/100°C	0.376	0.194	0.339	0.983	0.21	0.23	0.017	0.40	0.27	<0.02
18	9.59	10 hr/300°C	0.385	0.198	0.340	0.948	0.21	0.23	0.052	0.40	0.27	<0.02
18	9.59	1 hr/400°C	0.339	0.206	0.279	0.897	0.21	0.23	0.103	0.40	0.27	<0.02
18	9.59	8 hr/400°C	0.342	0.214	0.272	0.878	0.21	0.23	0.122	0.40	0.27	<0.02
18	9.59	1 hr/500°C	0.370	0.210	0.306	0.787	0.207	0.234	0.213	0.40	0.27	<0.02
18	9.59	6 hr/500°C	0.378	0.210	0.295	0.750	0.208	0.242	0.250	0.40	0.27	<0.02
18	9.59	1 hr/600°C	0.371	0.202	0.270	0.695	0.209	0.240	0.305	0.40	0.27	<0.02

isomer shift is given by the average position of those outer two lines.

The singlet S2 arises from isolated iron atoms in solid solution in α-Al at room temperature. In a sample containing 0.024 a/o Fe, Janot and Gilbert[11] reported the position of this singlet to the +0.34 mm/sec (with respect to pure α-Fe at room temperature). Nasu et al.[12] reported a position of 0.42 mm/sec in a rapidly quenched sample containing 0.01 a/o Fe. The value adopted here, 0.40 mm/sec, is very close to these values. The area fraction of S1 is obtained by assuming that any difference in area between the low velocity peak and high velocity peak is due to the presence of S1. Since quadrupole doublets have other sources of asymmetry, a sensible value of S1 is only obtained for less than about 1 a/o Fe. At higher Fe concentration the relative contribution of S1 to the total spectrum is small and outside the resolution of the experiment ($\approx$0.03 area fraction).

The singlet S1 represents iron in a compound Al-Fe phase with a near neighbor environment which gives a very small electric field gradient at the iron site. An example of such a near neighbor environment would be Fe in cubic lattice with identical atoms around the Fe. The doublet, D, represents iron in a compound Al-Fe phase with an asymmetric near neighbor which gives rise to an electric field gradient at the iron site. An example would be Fe atoms in a hexagonal lattice or iron atoms in a cubic lattice with one or two Fe

near neighbors and the remainder aluminum near neighbors. There is thus a doublet contribution from iron clusters in an α-Al matrix, from Fe in the globular "S" phase, from Fe in Al_6Fe, and from Fe in Al_3Fe. The doublet from each of these phases appears to overlap and hence these phases cannot be resolved from the doublet. However, the major contribution from the singlet S1 appears from Al_6Fe, with a much smaller contribution from both the "S" and Al_3Fe phases. Thus the amount of S1 present can be used to indicate the relative amount of Al_3Fe with complete conversion to Al_3Fe indicated when the S1 singlet comprises an area fraction of approximately 0.30.

b. Supersaturated Aluminum Matrix

The solid solubility of Fe in aluminum is known to be extremely small. According to Edgar[13] it reaches a maximum of 0.02 a/o at 640°C. Measurements using NGR to determine the solid solubility[14] have basically confirmed Edgar's result. Further measurements[15] using NGR and x-ray diffraction on alloys rapidly-quenched by a gun technique have shown that perhaps as much as 2 or 3 a/o Fe can be retained in the α-Al matrix. The NGR results shown in Fig. 35 (a)-(c) and Table 2 indicate that the melt spinning technique used here gives between 0.1 and 0.5 a/o Fe in supersaturated α-Al, in agreement with the TEM results on these same alloys. This is considerably more than the equilibrium amount, but less than

the amount achieved by the gun technique showing that the solidification rate achieved by the melt spinning technique used here is lower than that obtained by the gun technique used by Nasu, et al.[15]

c. Effect of Thermal Treatment

Alloys containing 18 w/o (9.59 a/o) Fe were subjected to a series of heat treatments. These were isothermal treatments, i.e., each heat treatment started with the as-spun alloy. The results obtained from an analysis of these spectra and the heat treatments given are shown in Table 2. Figure 37 plots the area fraction of the central peak (S1) as a function of annealing temperature. The area of this peak reflects the amount of Al_3Fe environment sensed by the iron atoms. When the area fraction of S1 reaches approximately 0.3, transformation to Al_3Fe is complete. In agreement with TEM results, no transformation is detected at 300°C and below. Also in agreement with the TEM results, the transformation to Al_3Fe is essentially complete for temperatures at and above 500°C. However, at 400°C the NGR detects only a partial transformation to Al_3Fe, in contrast to the TEM results at 400°C. This indicates that the Al_3Fe which forms at 400°C contains large numbers of defects which prevent the iron atoms from being in a symmetric environment on a microscopic scale.

5. Discussion

Of all the aluminum binary systems, rapidly solidified Al-Fe alloys are the most reported. However, the compositions studied are low in iron content. Examples are: up to 4.4 at% (16), 2 at% (17), up to 6 at% (18), 8 wt% (∿4 at%) (19), up to 6.1 wt% (∿3 at%)(10) and 0.5 wt% (0.24 at%) (20). H. Jones (7) investigated a wide variety of Al-Fe compositions, up to 32.9 wt% Fe (19.15 at%), but studied in the TEM only compositions up to 11 wt% (5.6 at% Fe). Jacobs and coauthors (19) analyzed the electron diffraction rings generated from an Al 8 wt% Fe alloy as representing a cubic phase with cell parameter of 0.0360 nm. Our study is able to confirm most of the reported rings, however, a detailed examination of our patterns, identical for the two compositions studied, shows more rings, some of which were not reported by Jacobs (19). Our x-ray diffraction analysis further confirmed the TEM diffraction patterns, and the results suggest that the structure of the globules and the cell boundaries in the aluminum matrix is more complex.

The disappearance of the globular phase and the formation of Al_3Fe needles suggests that there is no intermediate phase, and upon dissolving, the Al-18 wt% Fe does not form Al_6Fe.

Only three phases could be detected in all the alloys investigated, namely Al, Al_3Fe and an unidentified phase very

fine in shape which occurs in the cell boundaries and in the globular particles found in the alloys Al-10 wt% Fe, to Al-25.7 wt% Fe.

A hypothetical metastable phase diagram is shown in Fig. 38. The liquidus and solidus have been extended by dotted lines. It is known that the formation of Al_3Fe can be suppressed even at low cooling rates and Al_6Fe forms with the approximate eutectic temperature and composition shown. At the high solidification rates achieved in the melt-spun alloys, the formation of Al_6Fe is suppressed and "S" phase forms. The appearance of the primary globules of "S" phase in the microstructure above 12 w/o Fe suggests a possible metastable eutectic between liquid, α-Al, and "S" at ∿10.5 w/o Fe. Due to kinetic factors, such as an asymmetric coupled zone (common for Al-Fe alloys), this composition should be considered an upper bound. Between the metastable eutectic and 25 w/o Fe, the cellular and globular "S" are observed. Above 25 w/o Fe only globular "S" and Al_3Fe are observed in the melt-spun alloys. Further studies are underway to quantify the phases present, to determine the effect of heat treatment, and to extend the results with ternary additions.

Acknowledgements

We wish to thank F.S. Biancaniello for the preparation of alloys and W.J. Boettinger, J.L. Murray, and L.H. Bennett for valuable discussions.

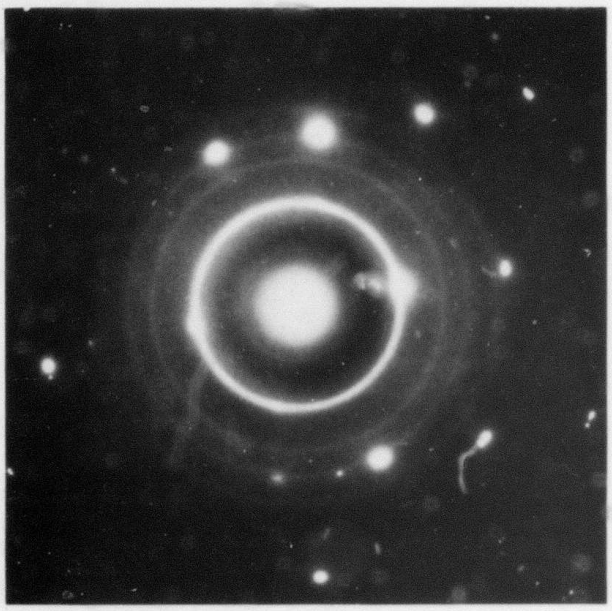

FIGURE 1.
Selected area diffraction pattern obtained from the intercellular "S" phase.

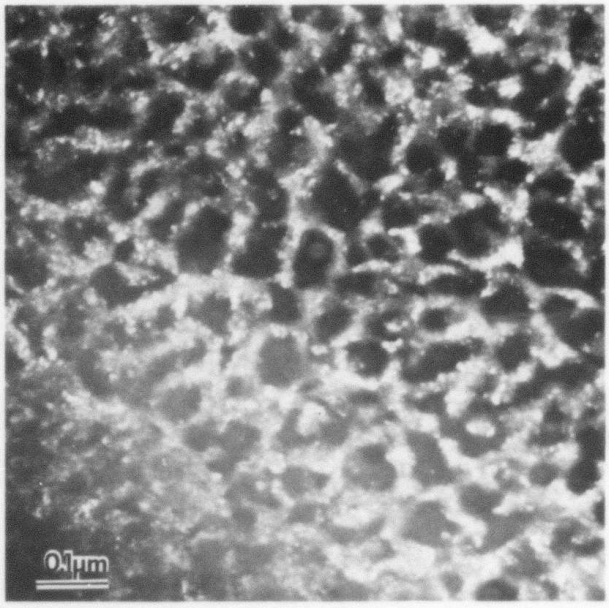

FIGURE 2.
The intercellular phase (dark field image) taken with the strongest ring of Figure 1.

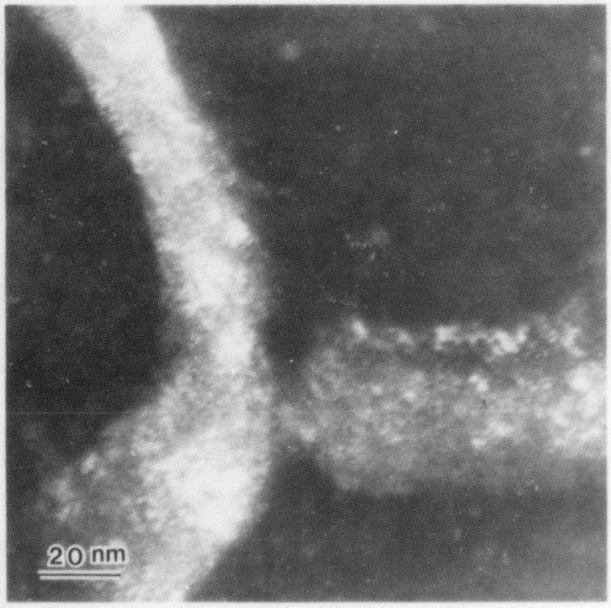

FIGURE 3.
The intercellular "S" phase is composed of fine particles (dark field image).

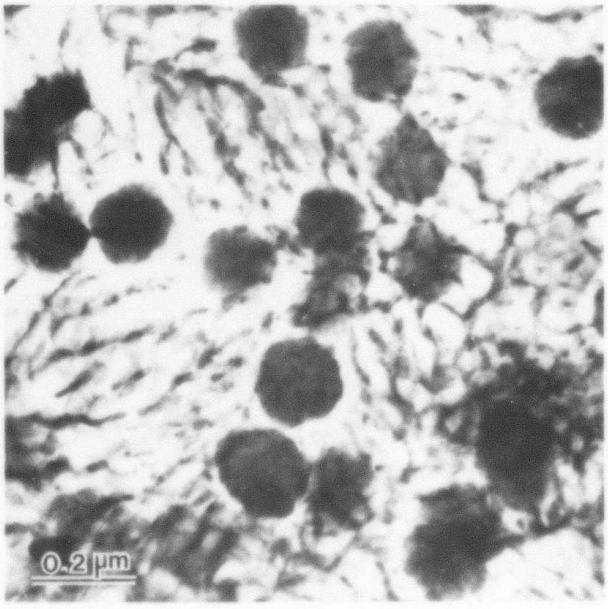

FIGURE 4.
The globular "S" phase in a cellular aluminum matrix.

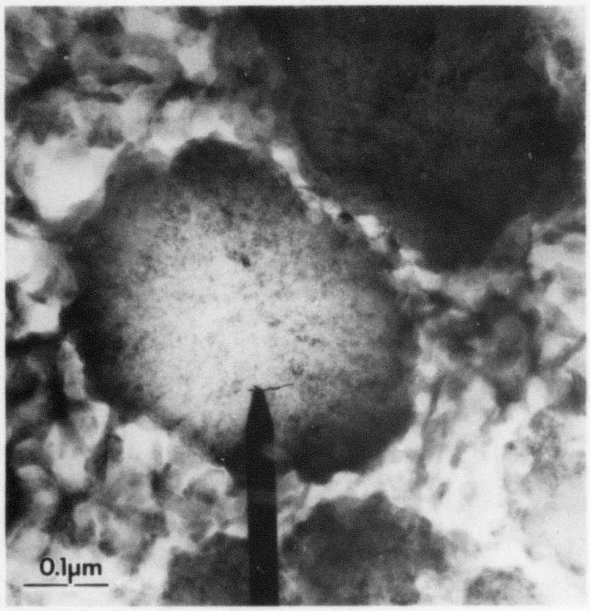

FIGURE 5.
The globular "S" phase (bright field image) showing fine details of the microstructure.

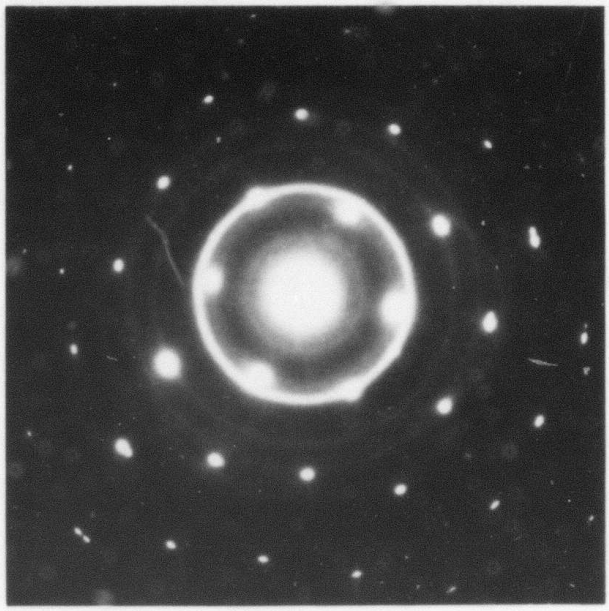

FIGURE 6.
Selected area diffraction pattern obtained from a globular "S" particle.

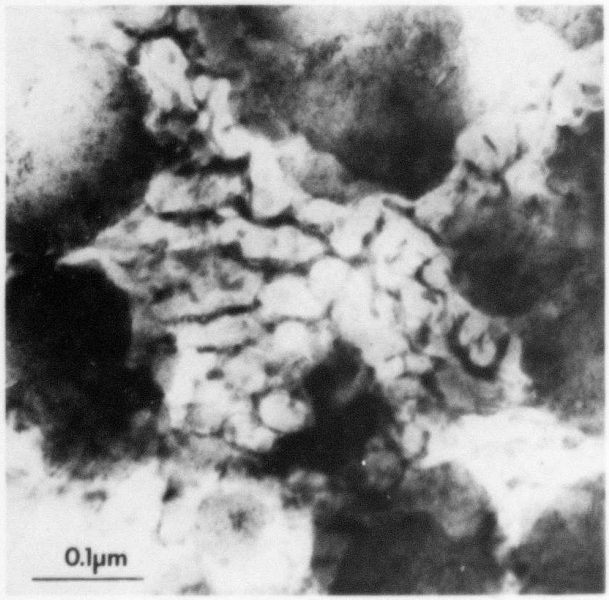

FIGURE 7.
Globular "S" phase in a cellular aluminum matrix (bright field).

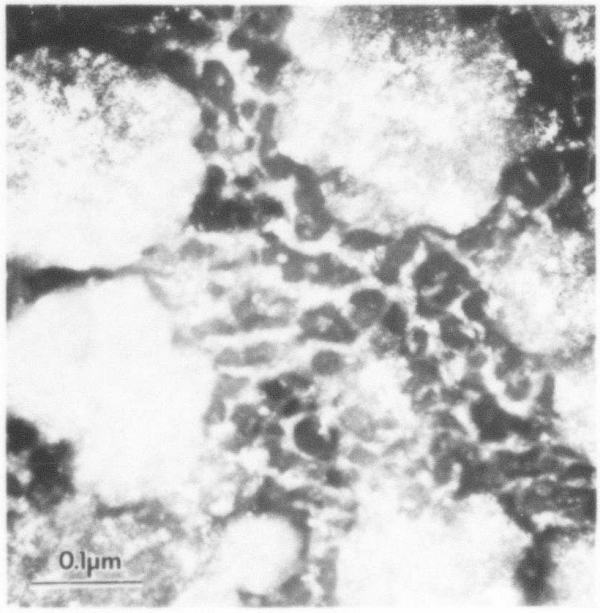

FIGURE 8.
Globular "S" phase in a cellular aluminum matrix (dark field) taken from the strongest ring. Note that both the globular and the intercellular "S" phase have the same contrast.

FIGURE 9.
Convergent beam diffraction pattern taken from a single crystal globular "S" phase.

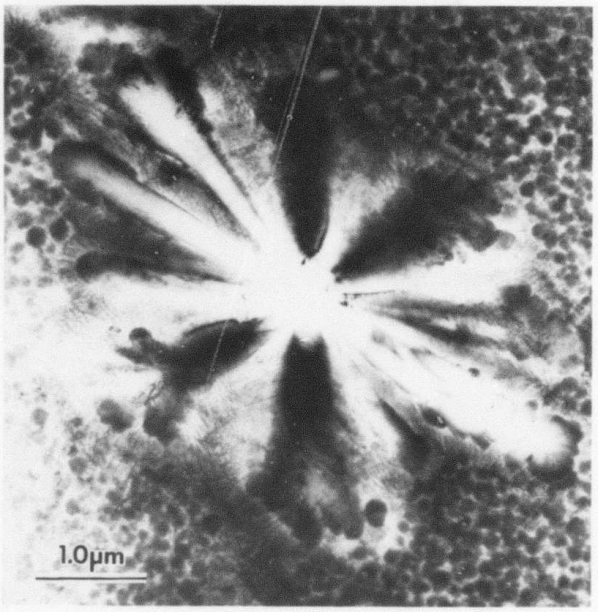

FIGURE 10.
The flower-like phase.

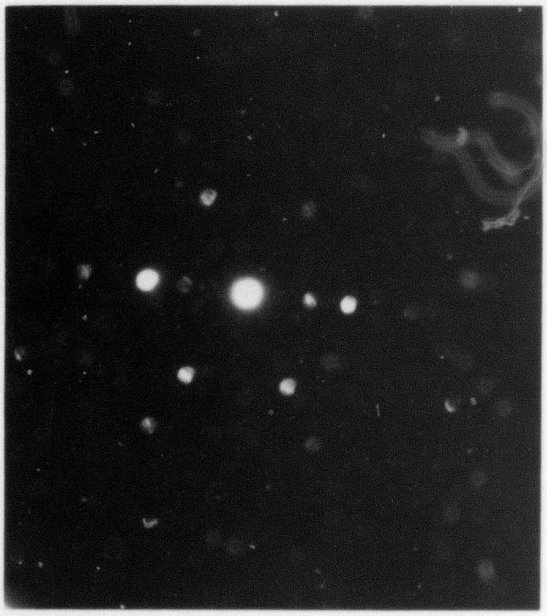

FIGURE 11.
Convergent beam diffraction pattern obtained from the flower-like phase.

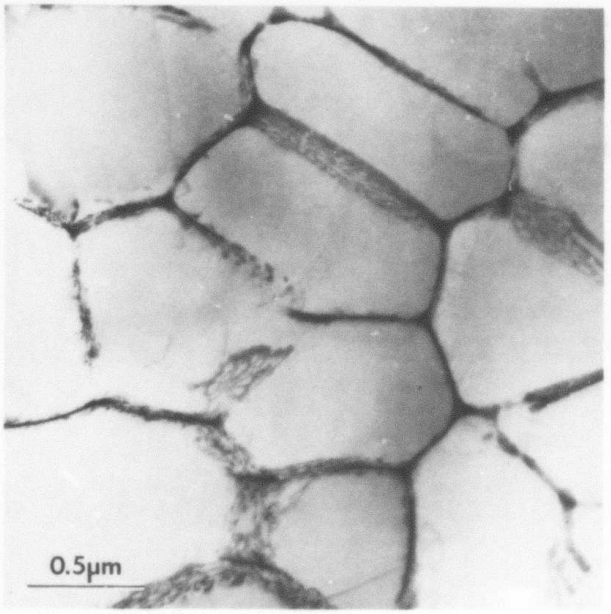

FIGURE 12.
Aℓ-1 wt.% Fe. Cellular aluminum containing networks of dislocations at the cell boundary.

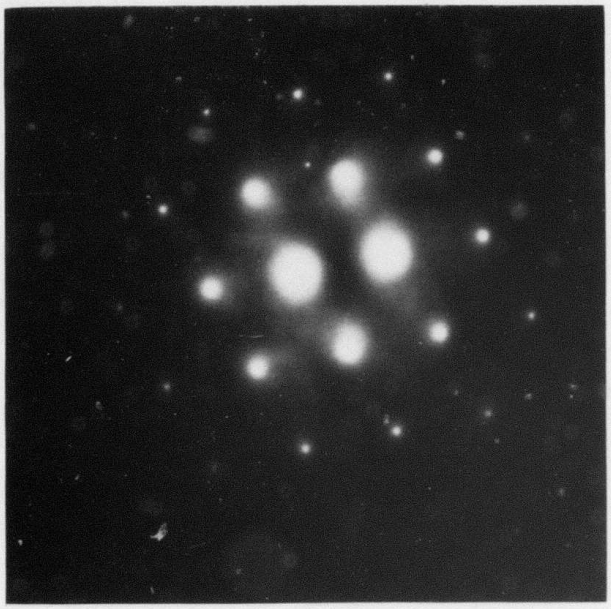

FIGURE 13.
Selected area diffraction pattern which shows no evidence of the small quantity of "S" phase at the cell boundary of the Aℓ-1 wt.% Fe.

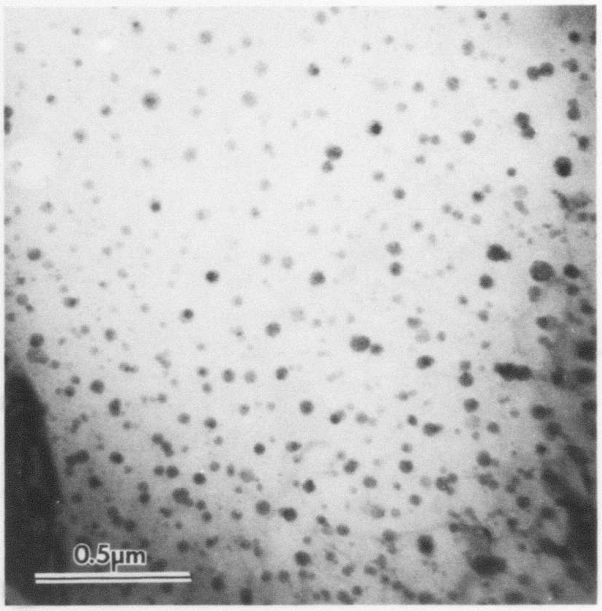

FIGURE 14.
Aℓ-1 wt.% Fe. Round particles are found in cell free regions of the foil.

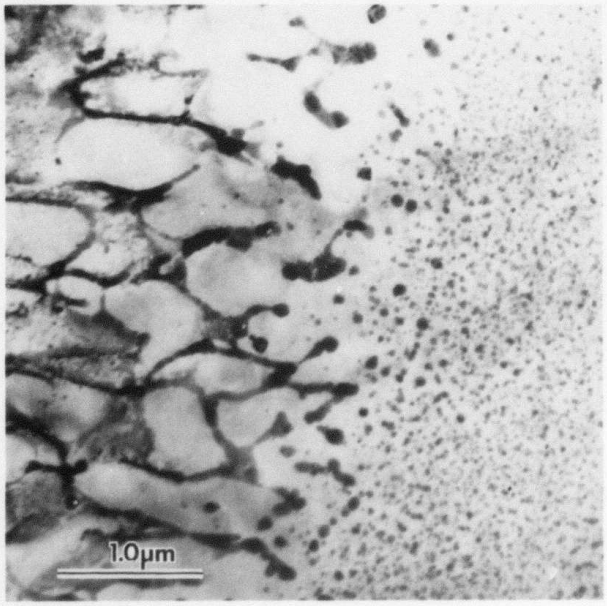

FIGURE 15.
Aℓ-2 wt.% Fe. A transition zone between a free microstructure on the right and a cellular microstructure on the left. May indicate the position in which the solidifying front (moving from right to left) reaches instability.

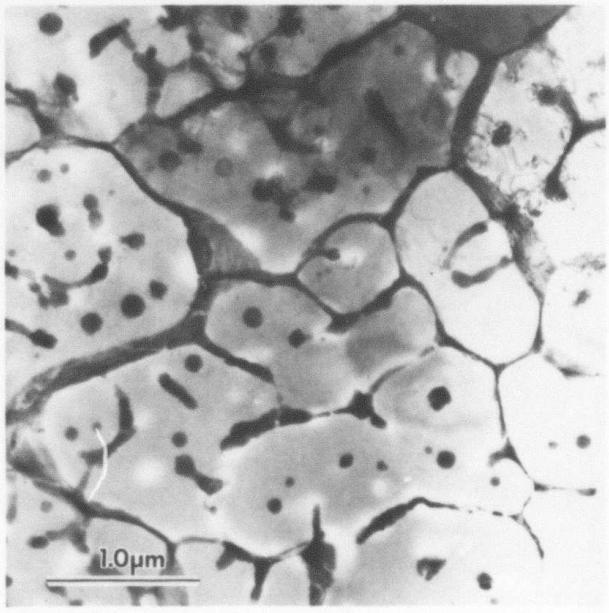

FIGURE 16.
Aℓ-3 wt.% Fe. In this cell formation the amount of the intercellular "S" phase is sufficient to diffract the electron beam (see Figure 17).

FIGURE 17.
Aℓ-3 wt.% Fe. Selected area diffraction pattern from the region shown in Figure 16. Note that diffraction ring originated from the cell boundaries.

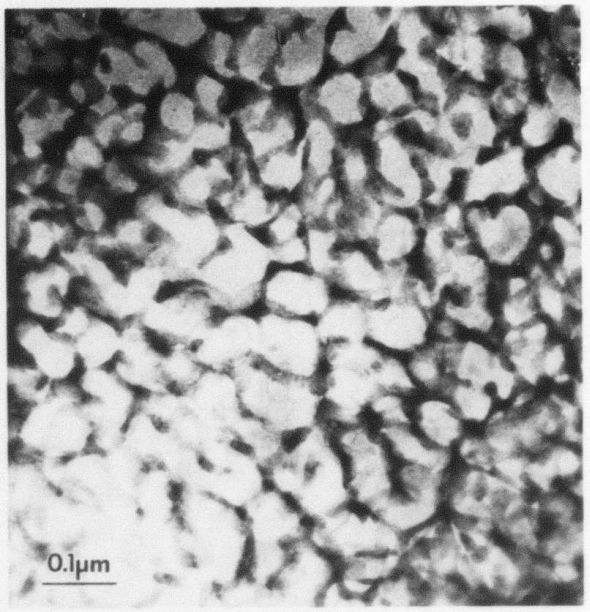

FIGURE 18.
Aℓ-9 wt.% Fe. Small cell (~ 0.1 μm) formation.

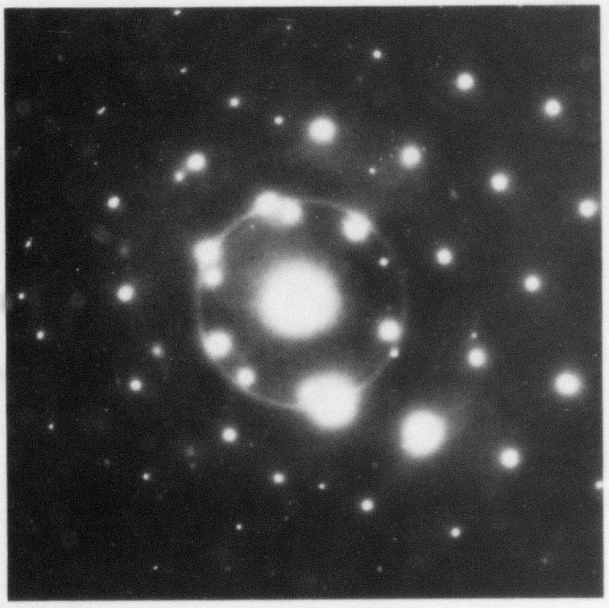

FIGURE 19.
Aℓ-9 wt.% Fe. Selected area diffraction pattern from region shown in Figure 18.

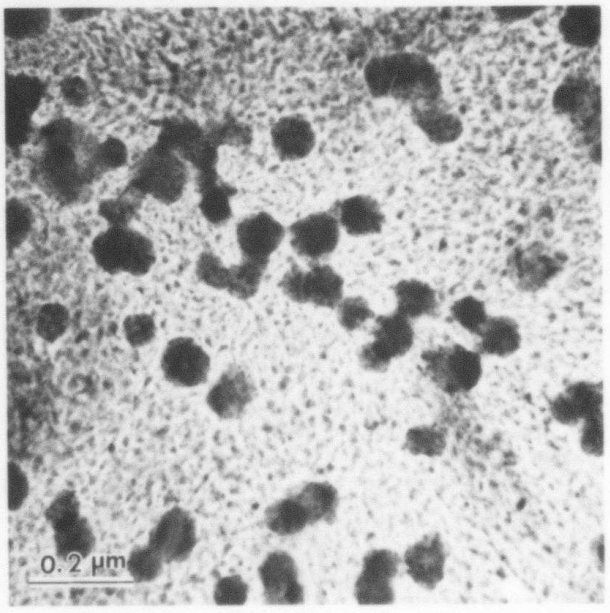

FIGURE 20.
Aℓ-10 wt.% Fe. Globular "S" in a cellular aluminum matrix.

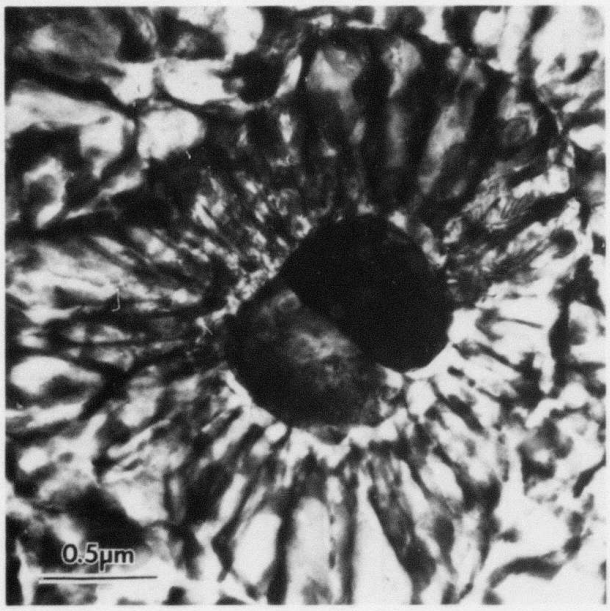

FIGURE 21.
Aℓ-11 wt.% Fe. Globular "S" particle serves as nucleation site for the cellular aluminum.

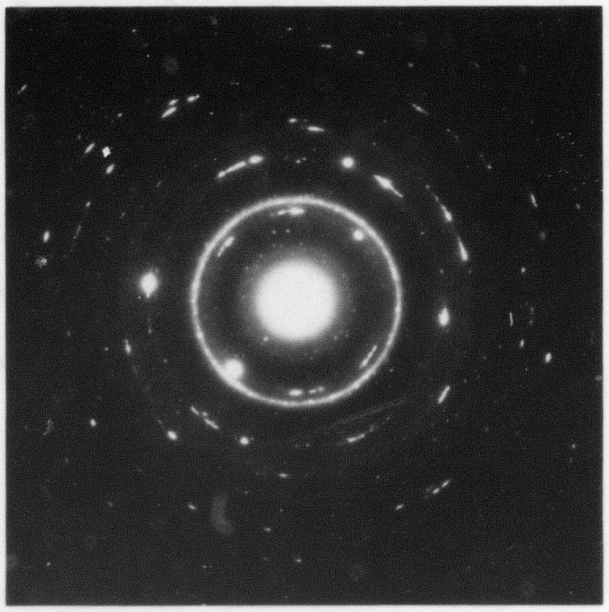

FIGURE 22.
Aℓ-12 wt.% Fe. Selected area diffraction pattern with rings originating from the "S" phase. Note discreteness of spots on rings, indicating larger crystals of the "S" phase than found in alloys of lower Fe content.

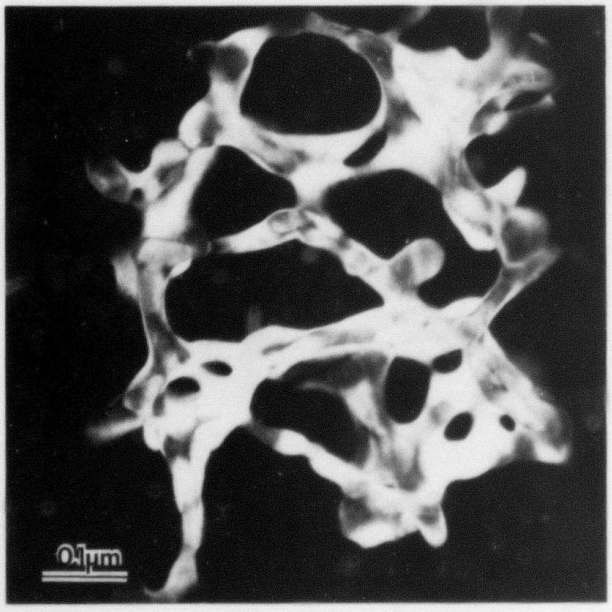

FIGURE 24.
Aℓ-16 wt.% Fe. In this alloy the "S" phase and the matrix sometimes grow as two interlocking systems. Dark field image of the "S" phase.

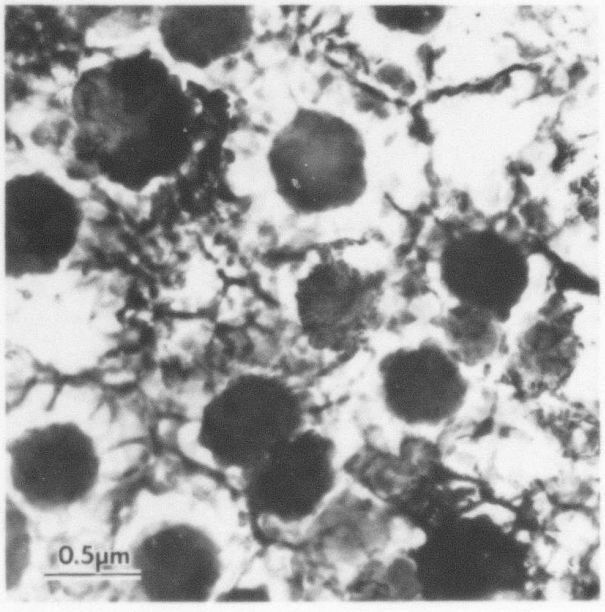

FIGURE 23.
Aℓ-12 wt.% Fe. The density and size of the globular "S" particles grow as the amount of Fe in the alloy increases.

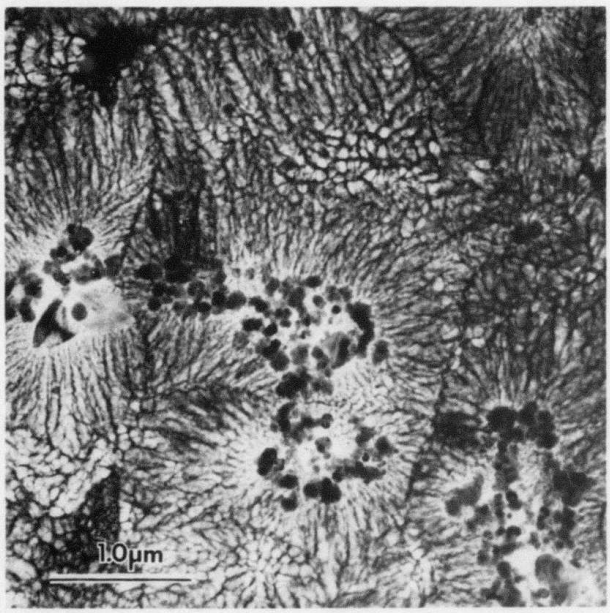

FIGURE 25.
Aℓ-16 wt.% Fe. "S" phase particle clusters serve as nucleation site for the cellular aluminum matrix.

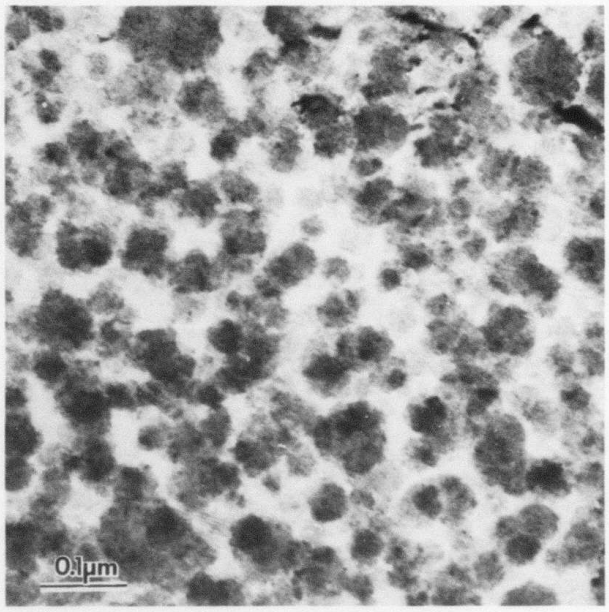

FIGURE 26.
Aℓ-18 wt.% Fe. The high density of the globular "S" particle prevent cell formation.

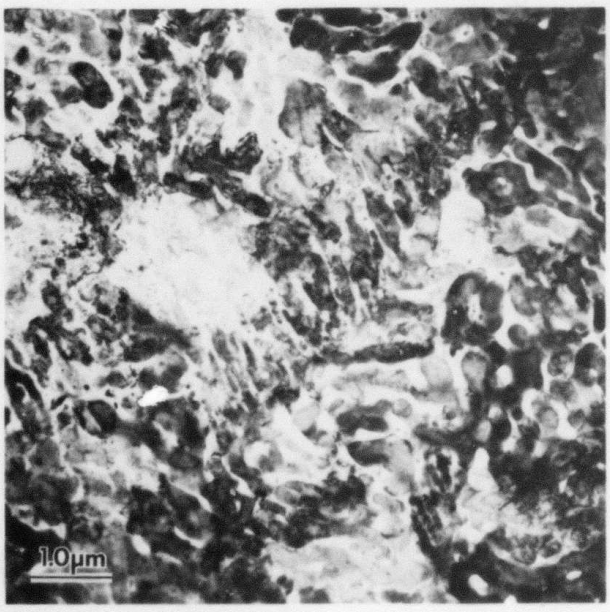

FIGURE 27.
Aℓ-25.7 wt.% Fe. The "S" phase occupies almost all the volume with aluminum solidifying in the spaces between the "S" particles.

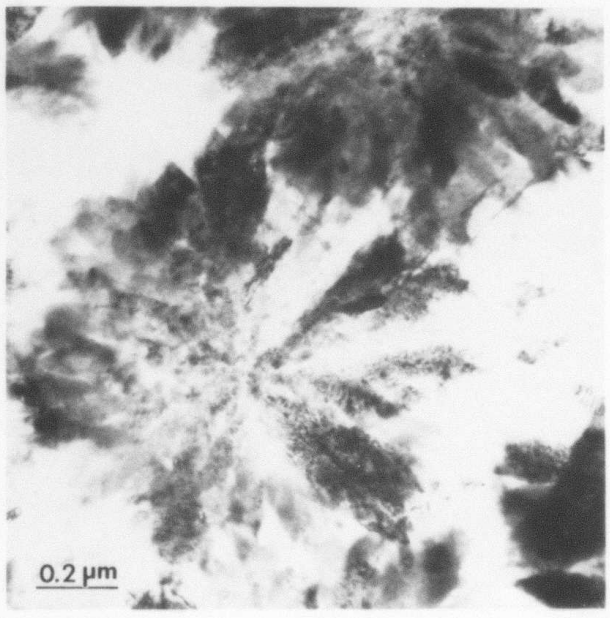

FIGURE 28.
Aℓ-25.7 wt.% Fe. In most cases the "S" particles have the characteristic cross-section shown here.

FIGURE 29.
Aℓ-34 wt.% Fe. $A\ell_3Fe$ is the only phase detected in this alloy.

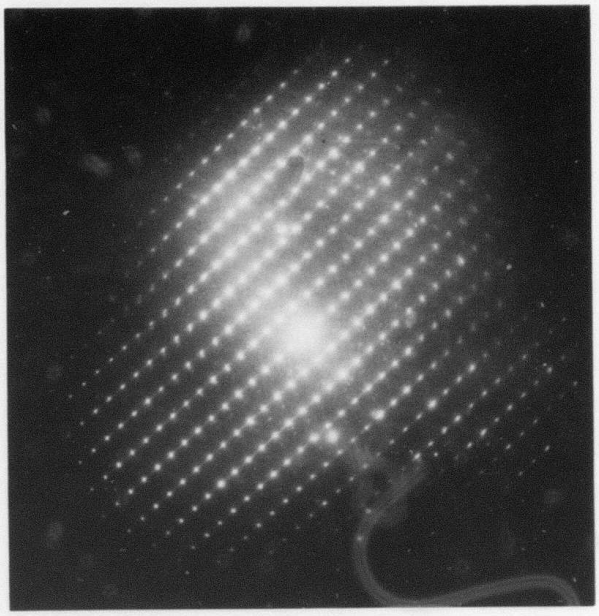

FIGURE 30.
Aℓ-34 wt.% Fe. Selected area diffraction pattern indicates that the structure is $A\ell_3Fe$.

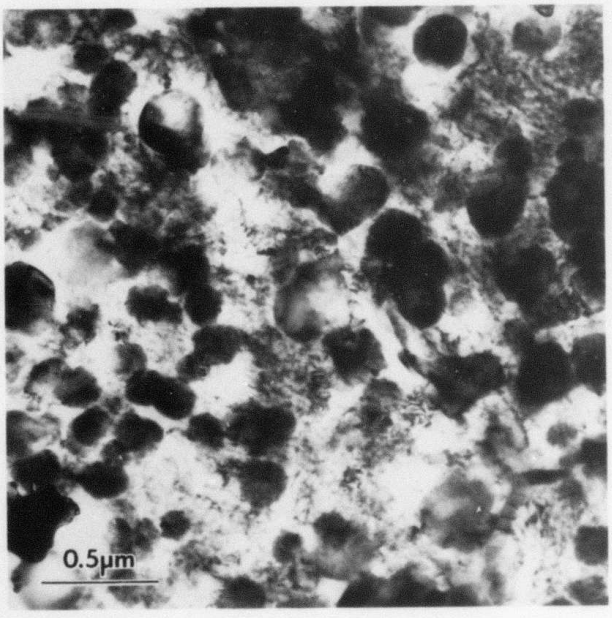

FIGURE 31.
Aℓ-18 wt.% Fe. Following 10 hours at 300°C, no morphological changes are observed, but the "S" particles crystallize into single crystals.

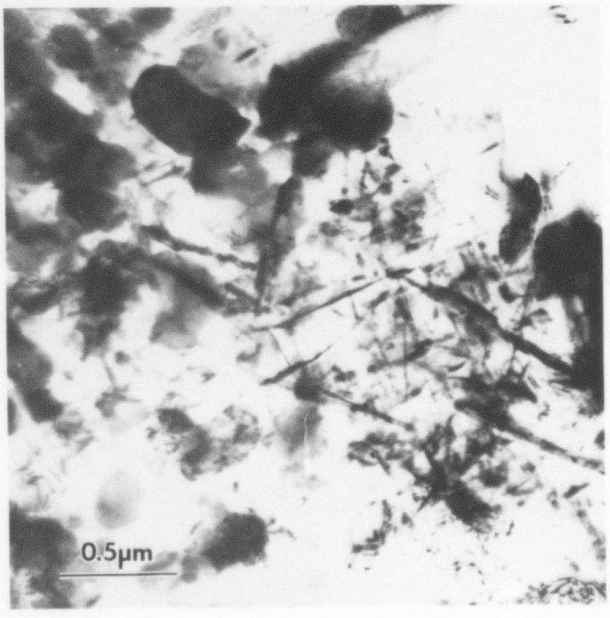

FIGURE 32.
Aℓ-18 wt.% Fe. Following 1 hour at 400°C rod-like $A\ell_3Fe$ particles can be observed in certain areas.

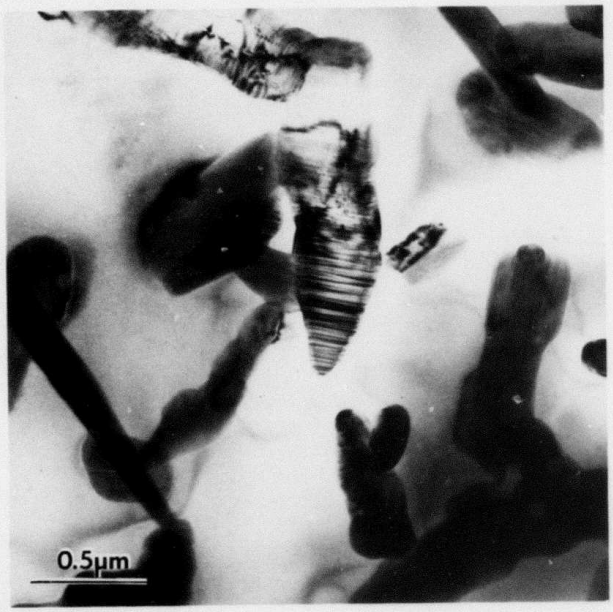

FIGURE 33.
Aℓ-18 wt.% Fe. Following 8 hours at 400°C, well developed $Aℓ_3Fe$ is seen reaching the length of over a micron.

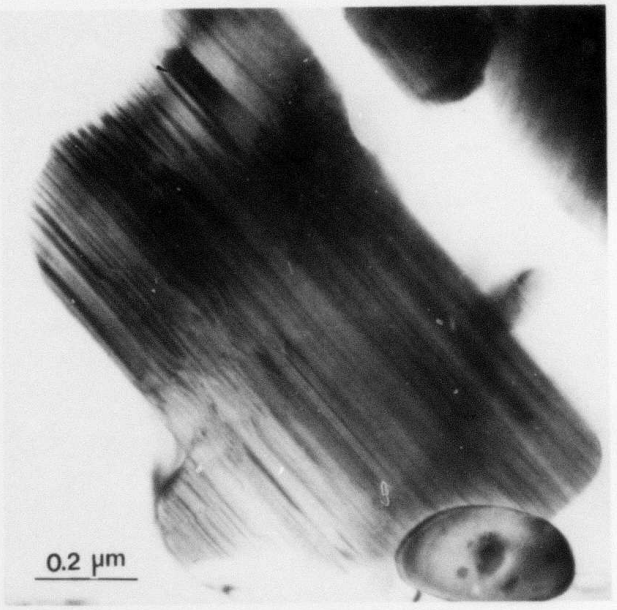

FIGURE 34.
Aℓ-18 wt.% Fe at 500°C for 6 hours. Characteristic striated $Aℓ_3Fe$ particles grow in length and width to well over a micron.

FIGURE 35. Nuclear gamma-ray resonance spectra from various melt-spun Al-Fe alloys. Positive velocities indicate source and absorber approaching each other. The zero of velocity is taken as the center of a spectrum from pure iron at room temperature. Each spectrum has been least squares fitted to three Lorentzian shaped lines. Data points are shown as data and the fitted spectrum as a solid line. The contribution from each of the three fitted lines is also shown as a solid line.

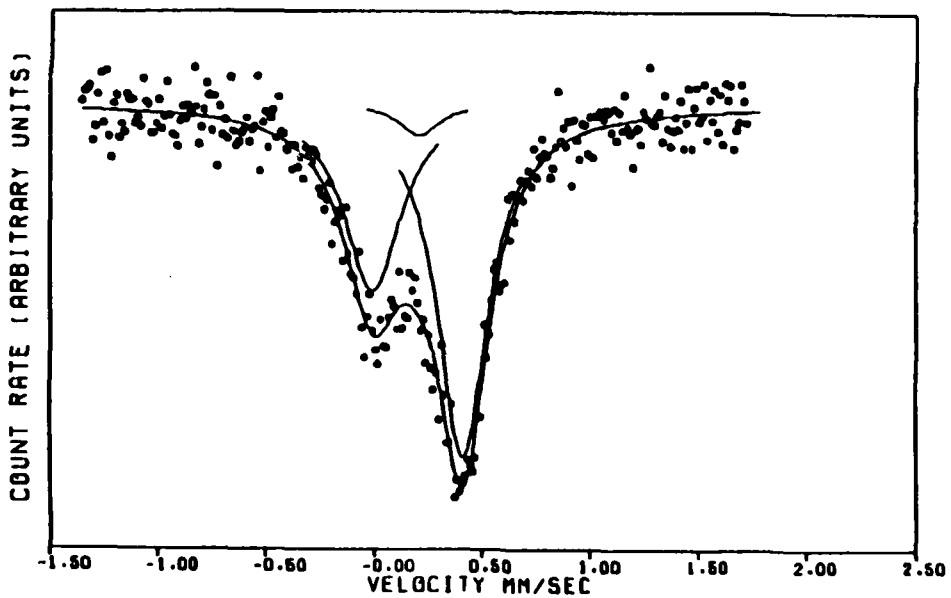

(a) 1 w/o Fe

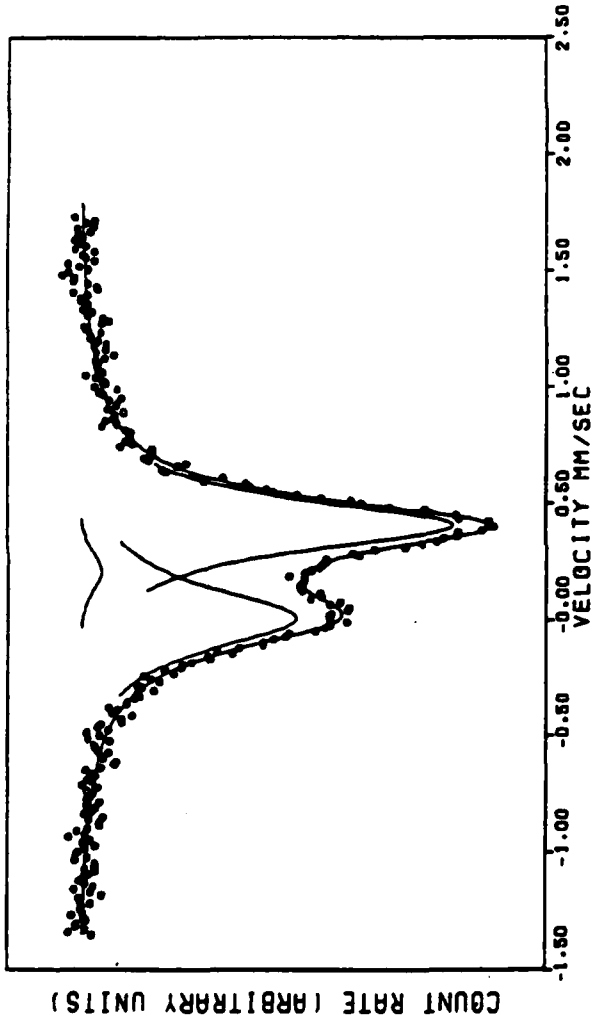

(b) 2 w/o Fe

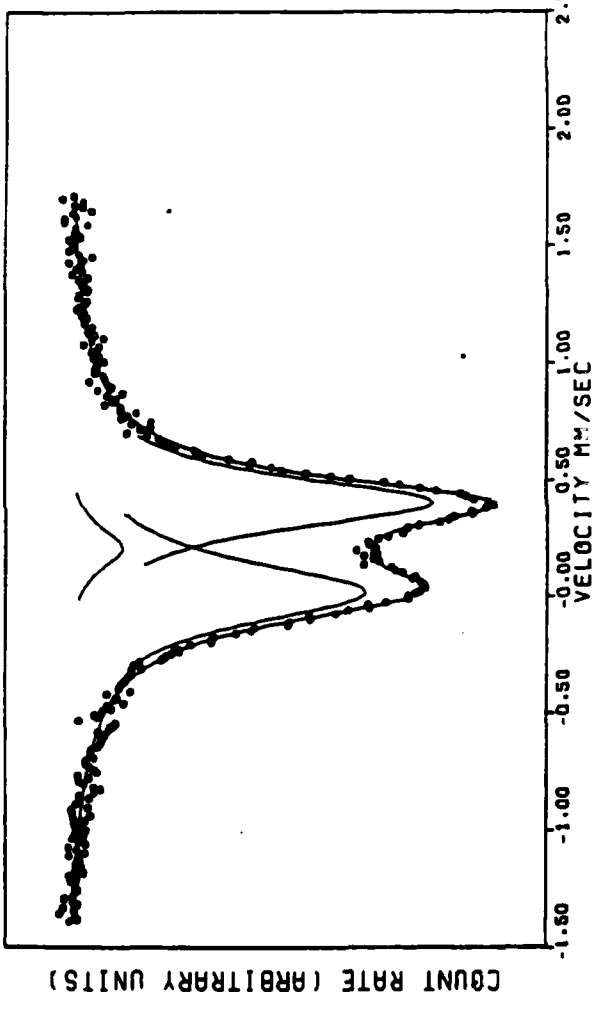

(c) 3 w/o Fe

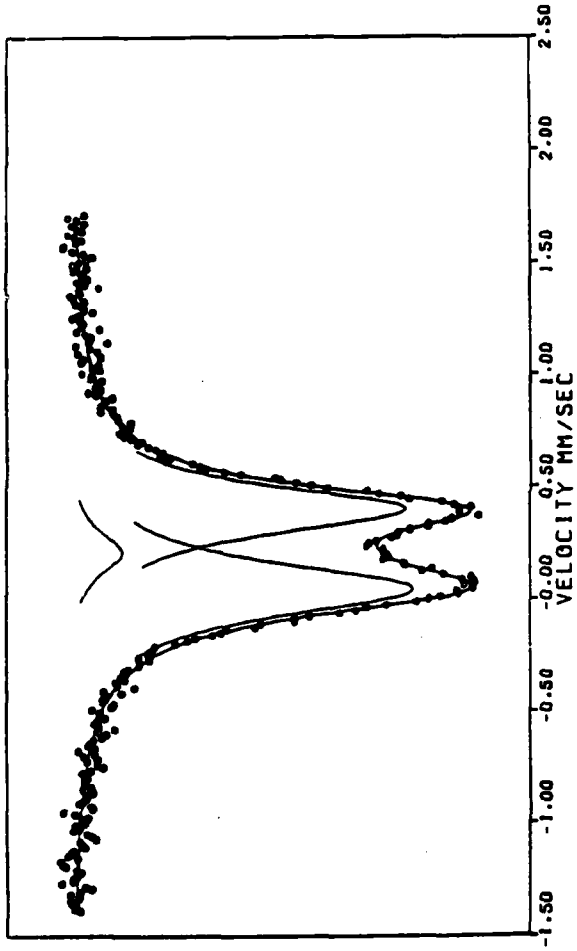

(d) 9 w/o Fe

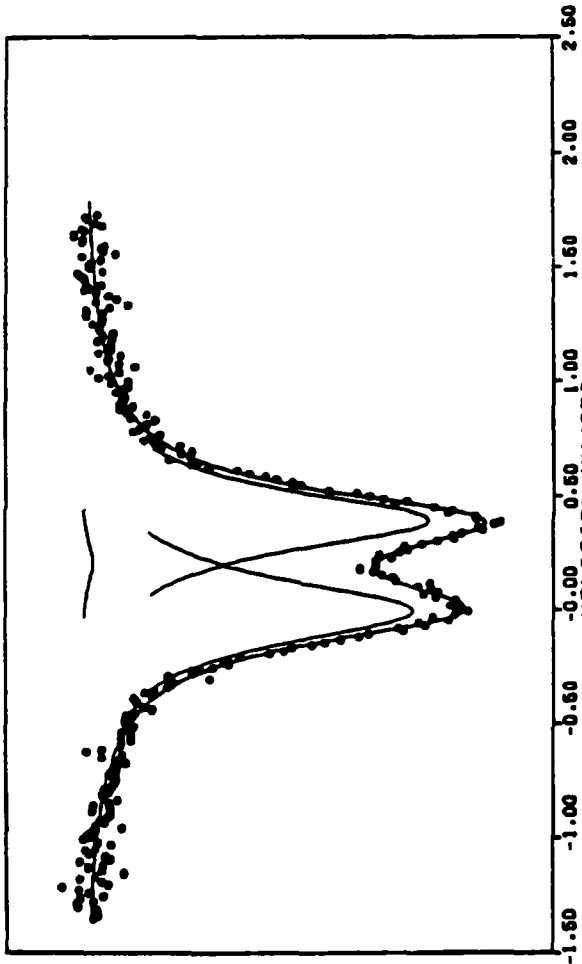

(e) 12 w/o Fe

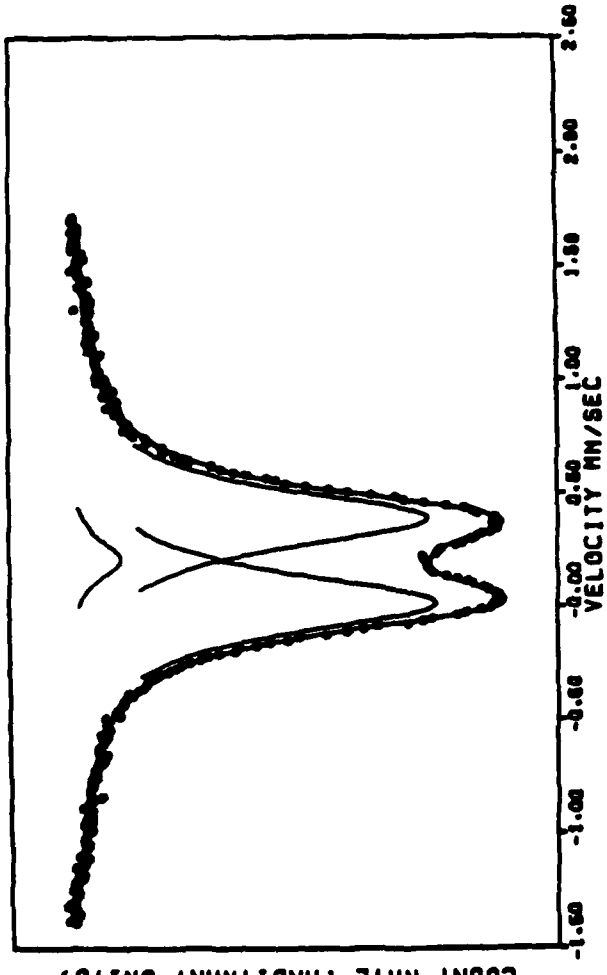

(f) 18 w/o Fe

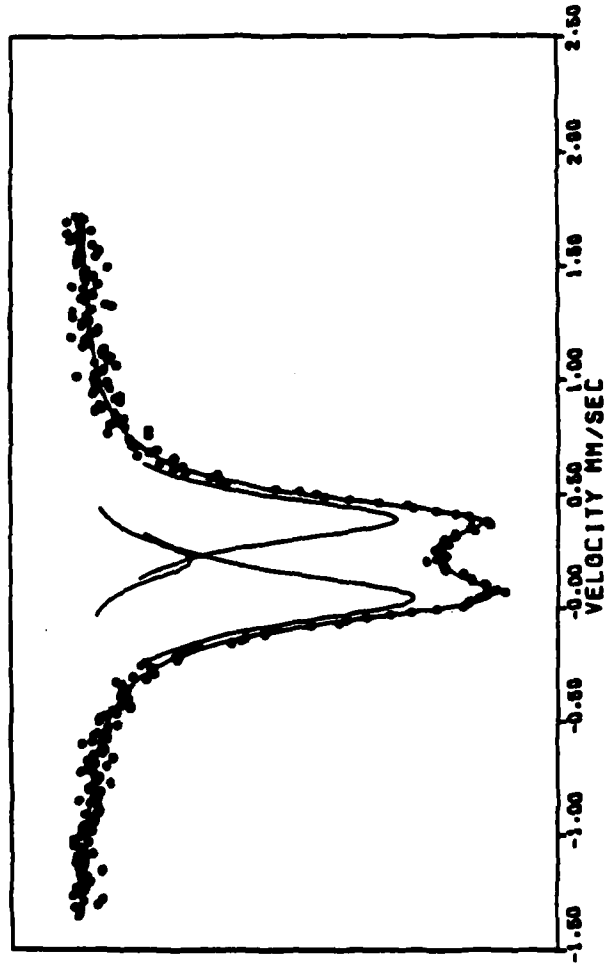

(g) 18 w/o Fe after 8 hours at 400°C

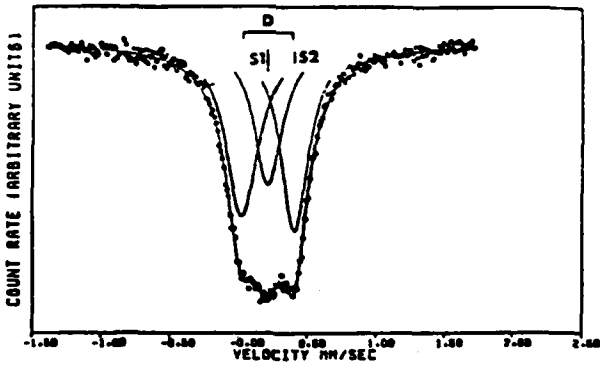

FIGURE 36. Nuclear gamma-ray resonance spectrum from a melt-spun sample of 34 w/o Fe. The spectrum has been analyzed as a symmetric doublet, D, a singlet S1, and singlet S2 (as in Figure 35). The marking shown indicates the position of the lines (but not their relative intensities).

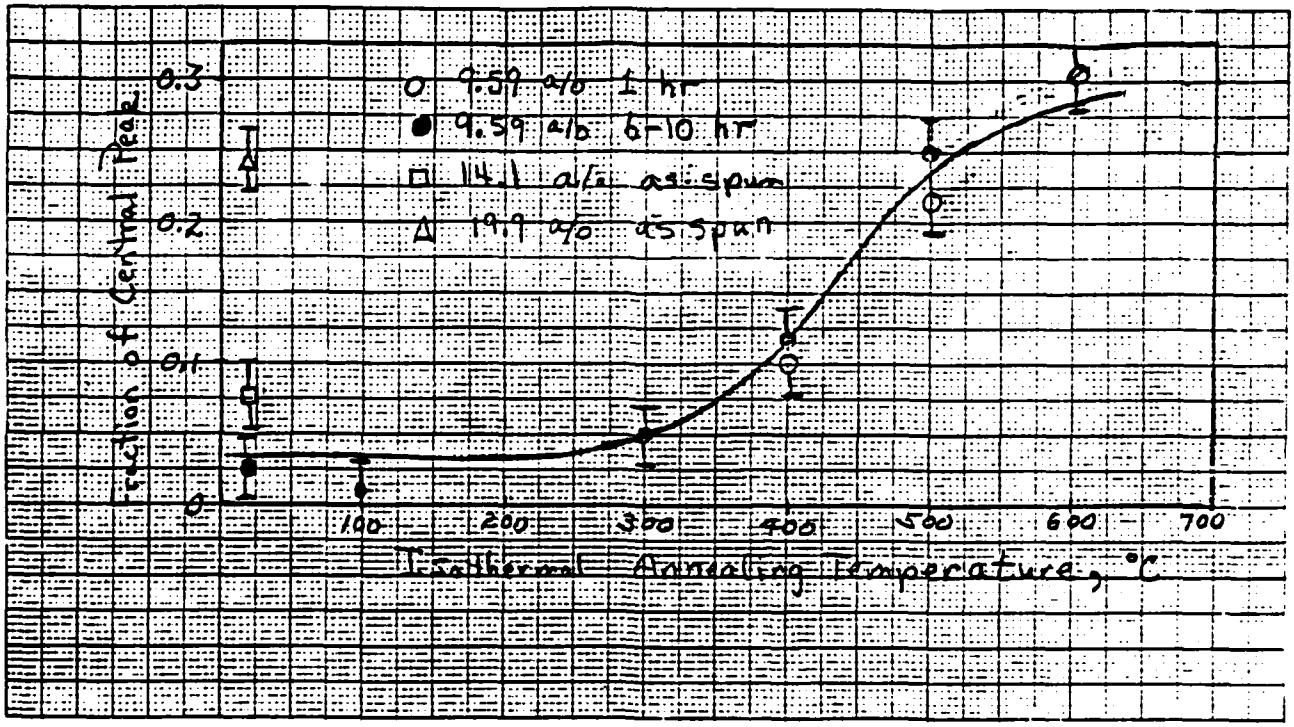

FIGURE 37. Area diffraction of the central NGR peak as a function of the isothermal annealing temperature for a melt-spun sample of 18 w/o (9.59 a/o) Fe. Open circles - annealed for 1 hour at the indicated temperature. Closed circles - annealed from 6 hours to 10 hours at the indicated temperature. Also shown are (square) an as-spun sample corresponding to the composition Al_6Fe and (triangle) an as-spun sample corresponding to the composition Al_3Fe.

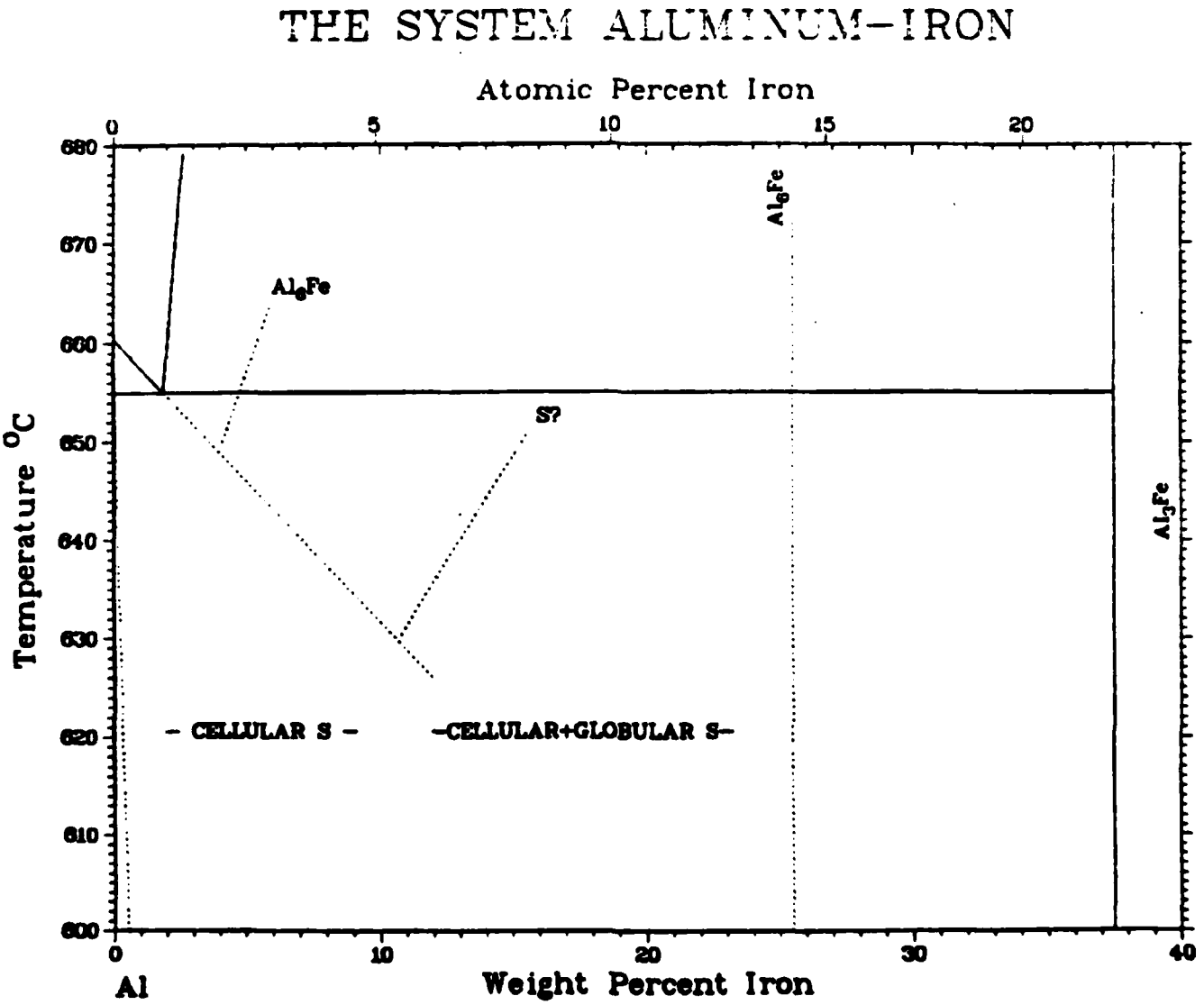

FIGURE 38. Phase diagram showing the estimated metastable liquidus for the "S" phase. The position shown represents an approximate upper limit for the metastable eutectic point of the S phase.

References

1. M. Hansen and K. Anderko, "Constitution of Binary Alloys," McGraw Hill, New York, 1958, p. 91.

2. E.H. Hollingsworth, G.R. Frank, and R.E. Willett, Trans AIME 234, 188 (1962).

3. L.K. Walford, Acta Cryst. 18, 287 (1965).

4. C.J. Simensen and R. Vellesamy, Z. Metallk. 68, 428 (1977).

5. L.R. Morris, "Solidification and Casting of Metals," The Metals Society, 1979, p. 218.

6. R.M.K. Young and T.W. Cline, Scripta Met. 15, 1211 (1981).

7. H. Jones, Mat. Sci. Engr. 5, 1 (1969).

8. I.R. Hughes and H. Jones, J. of Mat. Sci. 11, 1781 (1976).

9. T.R. Anantharaman, P. Ramachandrarao, C. Suryanarayana, S. Lele, and K. Chattapadhyay, Trans. Indian Inst. of Metals, 30, 423 (1977).

10. L.J. Swartzendruber and B.J. Evans, J. Catalysis 43, 207 (1976).

11. C. Janot and H. Gilbert, Phil Mag. 27, 545 (1973).

12. S. Nasu, U. Gonser, P.H. Shingu, and Y. Murikami, J. Phys. F. 4, L24 (1974).

13. J.K. Edgar, Trans AIME 180, 224 (1949).

14. S. Nasu and Y. Murakami, Phys. Stat Solidi (6) 46, 711 (1971).

15. S. Nasu, U. Gonser, P.H. Shingu, and Y. Murikami, J. Phys. F 4, L24 (1974).

16. A. Toneja and A. Bonefacia, J. Appl. Phys., 40 (1969), p. 419.

17. G. Blank, Z. Metallk., 63 (1972), p. 315.

18. P. Furrer and A.H. Warlimont, Z. Metallk. 64 (1973) p. 236.